Electronic Supplementary Material (ESI) for Sustainable Energy & Fuels.

Adaptation of $Cu(In, Ga)Se_2$ Photovoltaics for Full Unbiased Photocharge of Integrated Solar Vanadium Redox Flow Batteries

Sebastián Murcia-López,[1] Monalisa Chakraborty,[1] Nina M. Carretero,[1] Cristina Flox,[1] Joan R. Morante,[1,2] Teresa Andreu[1]*

1. Catalonia Institute for Energy Research (IREC), Jardins de les Dones de Negre 1, Sant Adrià de Besós, 08930, Spain

2. University of Barcelona (UB), Martí i Franquès 1, Barcelona, 08020, Spain

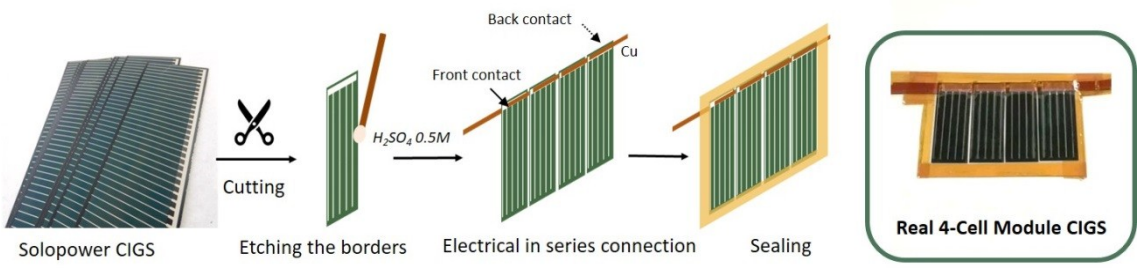

Figure S1. Scheme of the procedure for the CIGS mini-modules preparation.

Table S1. Comparative of fabrication cost for different thin film PV technologies versus multicrystalline Si.

Photovoltaic technology	Cost
Multicrystalline Silicon	Levelized cost of energy: 0.51 US$/$W_{DC}$[a] Minimum sustainable pricing: 0.27-0.36 US$/$W_{DC}$[b]
CIGS	Levelized cost of energy: 0.4 US$/$W_{DC}$ [a] with potential decrease to 0.22 US$/$W_{DC}$ in next gen fabrication (larger area). Minimum sustainable pricing: 0.4 – 0.5 US$/$W_{DC}$[b]
CdTe	Minimum sustainable princing: 0.35-0.45 US$/$W_{DC}$[b]

[a]White Paper for CIGS Thin Film Solar Cell Technology, Zentrum für Sonnenenergie- und Wasserstoff-Forschung Baden-Württemberg, Stuttgart (2015).
Available at: http://cigs-pv.net/wortpresse/wp-content/uploads/2015/12/CIGS-WhitePaper.pdf

[b]NREL: An Analysis of the Cost and Performance of Photovoltaic Systems as a Function of Module Area. Technical Report NREL/TP-6A20-67006 (2017).
Available at: https://www.nrel.gov/docs/fy17osti/67006.pdf

Battery evaluation under galvanostatic conditions:

Prior to the integration with the photovoltaic modules, electrochemical tests with the full cell were conducted, in order to validate the galvanostatic charge-discharge process and determine the operating voltages of the system. The cell was assembled as described previously, with 10 cm^2 H-TiO_2/CF and CF electrodes in the negative and positive sides, respectively. The cycling was conducted at constant current densities (10 and 20 $mA \cdot cm^{-2}$) and the cell voltage was followed in order to control the charge/discharge of the battery. Additionally, a reference electrode was put inside the cell so that the individual voltages in the positive (E_p) and negative (E_n) sides could be followed.

The obtained curves during galvanostatic cycling are presented in Figure S2, including the E_p, E_n and E_{cell} during the charge/discharge at different current densities. Despite the small decrease in the capacity seen at higher current densities, the battery provides acceptable efficiency and electrolyte utilization values (Table S2). As expected, the voltage efficiency decreases with the increase in the current density, although the coulombic efficiency is positively affected. The individual half-cell potentials, however, show certain unbalance between both sides: during charge, the E_p plainly increases indicating the positive side is fully charged, so that all available VO^{2+} has been oxidized to VO_2^+ and parasitic reactions such as oxygen evolution might start, while the potential in the negative side, E_n, is still decreasing, indicating that unreacted V^{3+} species are still present. The opposite situation is observed during the cell discharge: the non-fully charged negative side is discharged before the positive as seen by the steep decrease in the E_n. A more detailed analysis of these potentials shows, for instance, that the negative side starts to charge at ~-0.26 V_{SHE}, which is in good agreement with the thermodynamic potential for this half-reaction. The positive side, on the contrary, starts charging at ~1.12 V_{SHE}, which implies overpotentials that might be associated to ohmic losses in the cell, especially in the membrane.

Energy efficiencies of 80-76% are obtained for the galvanostatic charge at 10 and 20 $mA \cdot cm^{-2}$, respectively. Although slightly higher values have been reported for other VRFB with H-TiO_2/CF electrodes in the negative side and evaluated at similar current density,[28] the lower vanadium concentration used in the present study and some fluidic aspects regarding the use of different cell configurations account for the minor efficiency decrease.

Besides the efficiency values, as seen by the potential profile during the charge, at lower current density, the cell potential varies between 1.3 V in the discharged cell up to 1.8 V for the fully charged one. At higher current densities, the voltage efficiency decreases and the initial charging potential increases up to around 1.45 V. Clearly, as previously stated, an unbiased photocharge can only be achieved with a PV system providing these voltages working at similar current densities.

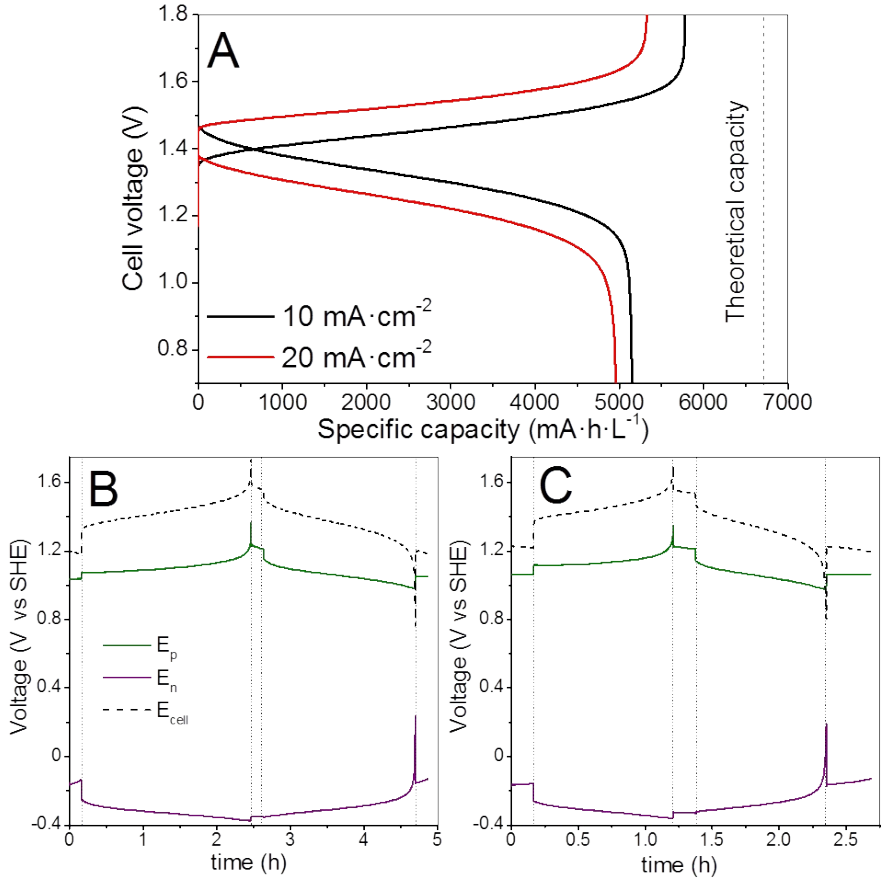

Figure S2. Charge/discharge profiles during the full cell measurements under galvanostatic conditions. Variation of the cell potential vs capacity during charge/discharge at different current densities (A); individual potentials in the positive (E_p) and negative (E_n) sides (V vs SHE), and estimated E_{cell} (V), during charge/discharge at 10 (B) and 20 mA·cm^{-2} (C). The CF electrodes have a geometrical area of 10 cm^2.

Table S2. Estimated efficiencies values and electrolyte utilization for the galvanostatic cycling of the cell.

Current density / mA·cm^{-2}	Coulombic efficiency (%)	Voltage efficiency (%)	Energy efficiency (%)	Electrolyte utilization (%)
10	89	90	80	77
20	93	82	76	74

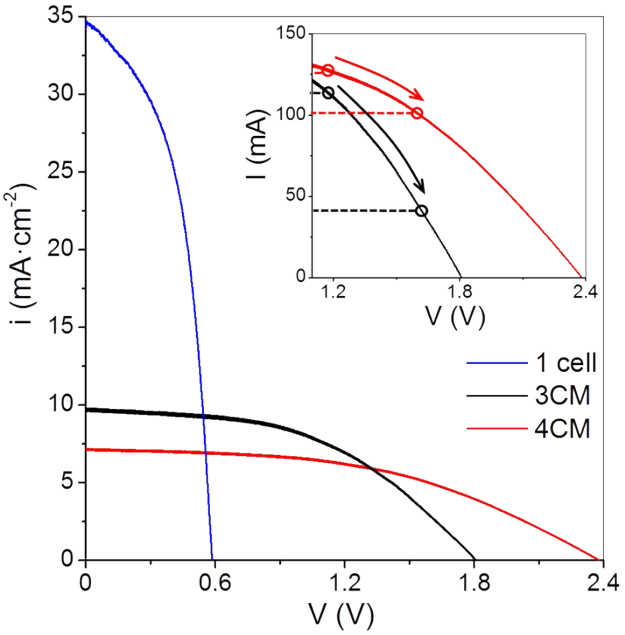

Figure S3. i-V characteristic curves of the CIGS modules under 1 Sun irradiation. In the inset, the operation region during a photocharge (1.2-1.6 V).

Table S3. Estimated solar cell efficiencies, fill factors, open circuit voltages (V_{OC}) and voltages at the maximum power point (V_{mp}) under AM1.5G illumination at 1 Sun, with the different CIGS modules.

CIGS Module	η (%)	FF (%)	V_{OC} (V)	V_{mp} (V)
1 cell	10.3	50	0.6	0.4
3CM	8.4	48	1.8	1.2
4CM	8.1	48	2.4	1.5

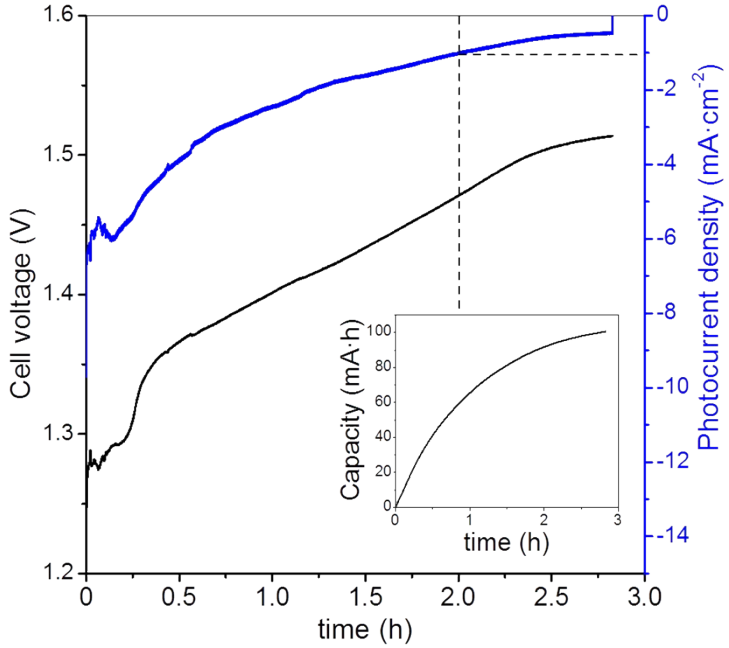

Figure S4. Cell voltage (black) and photocurrent density (blue) evolution during the photocharge of the full VRFB with the integrated 3CM under 1 Sun illumination. The battery was cycled with 10 mL of catholyte and anolyte.

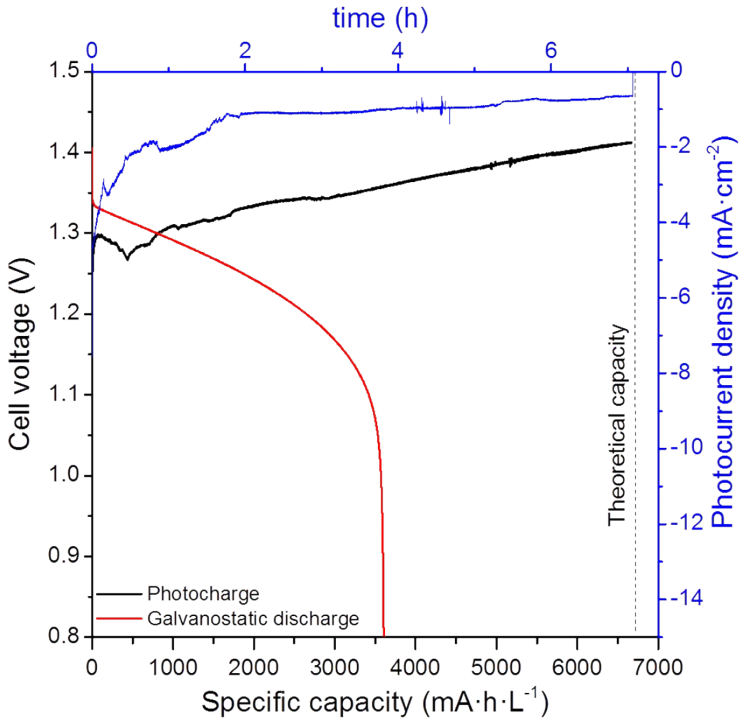

.

Figure S5. Cell voltage (black) and photocurrent density (blue) evolution during the photocharge of the full VRFB with the integrated 3CM under ~0.5 Sun illumination. The battery was cycled with 10 mL of catholyte and anolyte.

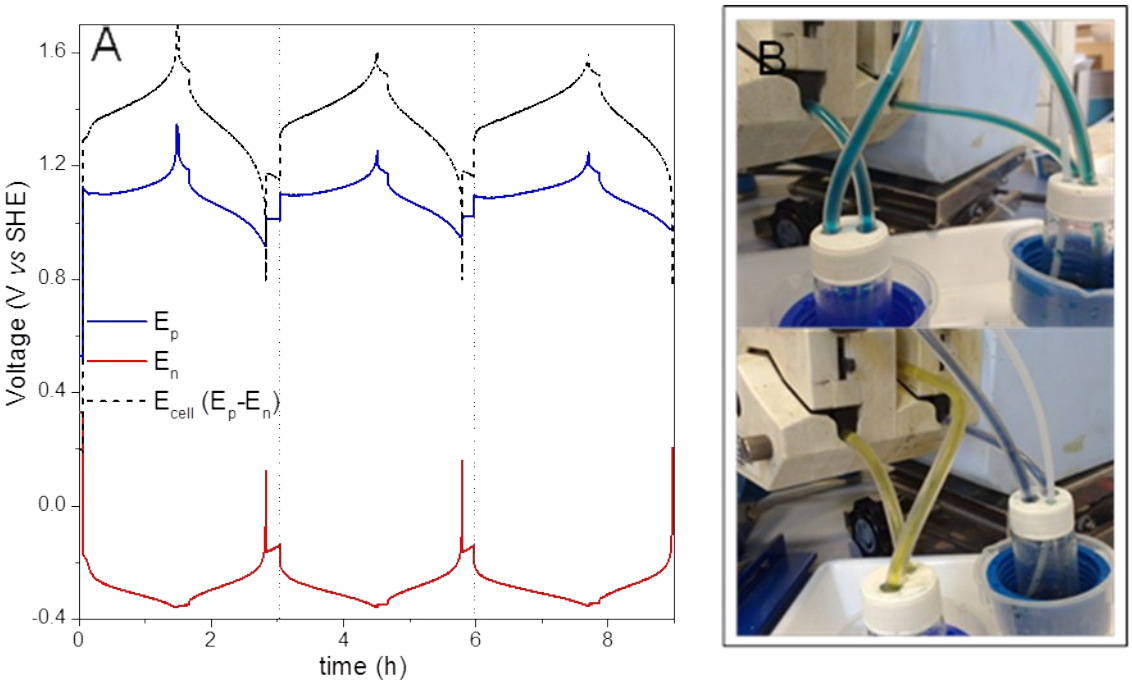

Figure S6. Evolution of the E_p, E_n and E_{cell} (followed by the reference electrode) during the photocharge/discharge with the 4CM (A), and variation of the electrolytes' colors before (up) and after (down) photocharge.

Table S4. Estimated efficiencies and discharge electrolyte utilization for the different VRFB.

Configuration	CE (%)	VE (%)	EE (%)	Electrolyte utilization (%)
3CM	52	90	47	38
4CM (cycle 2)	85	90	77	74
Galvanostatic@10 mA·cm^{-2}	89	90	80	77

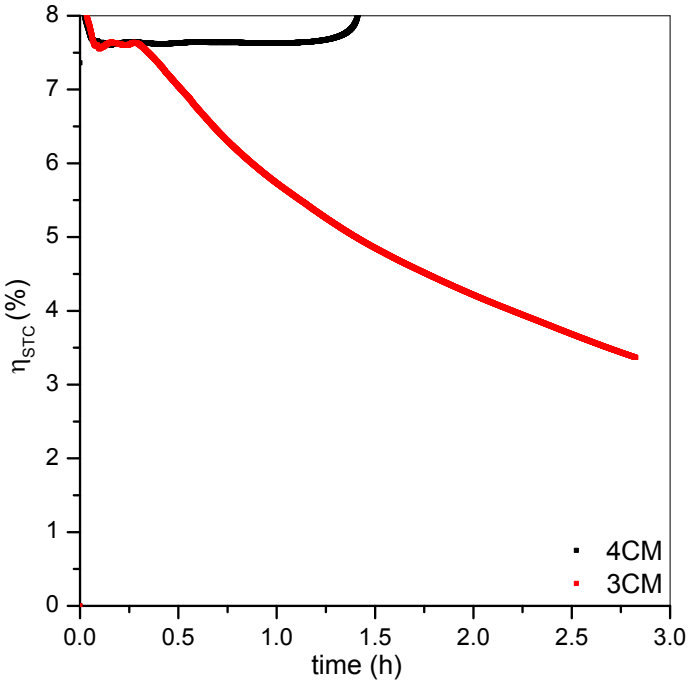

Figure S7. Variation of the η_{STC} during the photocharge of the full VRFB configuration with the 3CM and 4CM.

Table S5. Comparative table of several solar redox flow batteries

Type of battery	Photoelectrode/ photovoltaics	η (%)	η_{RT} (%)	Energy	Reference
Organic/inorganic (AQS-iodide)	WSe_2	-	2.8	Discharge cell voltage: 0.355 V ~0.06 mW·h[a]	11
Organic/inorganic (AQDS-bromide)	c-Si	-	3.2	Discharge cell voltage: 0.78V ~0.36 W·h·L^{-1}[a]	9
Organic (4-OH-TEMPO/ $MVCl_2$)	III-V tandem cell	26.1	14.1	Cell voltage: 1.25 V ~0.3 W·h·cm^{-2}·L^{-1}[a]	27
Organic (DHAQ/$K_4Fe(CN)_6$)[b]	Ta_3N_5 – GaN/Si	-	3.0[c]	0.2 W·h·L^{-1}	12
VRFB	TiO_2 photoanode	-	0.6[d]	-	19
VRFB	Triple junction TF Si	13.5[e]	8.5[a,e]	23 W·h·L^{-1} [e]	18
VRFB	Commercial CIGS (4 junctions)	8.1	5.0	6.25 W·h·L^{-1}	This work

[a]Value calculated from the i-t discharge curve.

[b]Static redox battery.

[c]Value calculated with respect to the operation photocurrent during charge and assuming 100% Faradaic efficiency for each half-reaction.

[d]Value calculated by estimating a 90% efficiency of discharge.

[e]At 300mW·cm^{-2} of illumination intensity.